NAVAL POSTGRADUATE SCHOOL
Monterey, California

THESIS

FINITE ELEMENT ANALYSIS OF SMART STRUCTURES AND MODAL TESTING OF A FLEXIBLE SPACECRAFT ARM

by

James C. Trump

December 1994

Thesis Advisor: Brij N. Agrawal

Approved for public release; distribution is unlimited

REPORT DOCUMENTATION PAGE

Form Approved OMB No. 0704

1. AGENCY USE ONLY *(Leave blank)*	2. REPORT DATE December 1994	3. REPORT TYPE AND DATES COVERED Master's Thesis

4. TITLE AND SUBTITLE
FINITE ELEMENT ANALYSIS OF SMART STRUCTURES AND MODAL TESTING OF A FLEXIBLE SPACECRAFT ARM

5. FUNDING NUMBERS

6. AUTHOR(S)
Trump, James C.

7. PERFORMING ORGANIZATION NAME(S) AND ADDRESS(ES)
Naval Postgraduate School
Monterey CA 93943-5000

8. PERFORMING ORGANIZATION REPORT NUMBER

9. SPONSORING/MONITORING AGENCY NAME(S) AND ADDRESS(ES)

10. SPONSORING/MONITORING AGENCY REPORT NUMBER

11. SUPPLEMENTARY NOTES The views expressed in this thesis are those of the author and do not reflect the official policy or position of the Department of Defense or the U.S. Government.

12a. DISTRIBUTION/AVAILABILITY STATEMENT Approved for public release; distribution unlimited

12b. DISTRIBUTION CODE

13. ABSTRACT *(maximum 200 words)*

This thesis deals with analytical predictions and experimental determination of the modal frequencies and shapes associated with the arm portion of the Naval Postgraduate School's Flexible Spacecraft Simulator (FSS). A description of how piezoceramic sensors and actuators are incorporated in finite element modeling is presented. A MATLAB™ code conducting the finite element modeling of the arm is used to verify the modal frequencies generated via Structural Dynamic Research Corporation's I-DEAS™ software. Modal testing is conducted with the I-DEAS Test package to determine the first four physical modal frequencies and shapes so that we may compare them with the analytical results. The results of the testing indicated that finite element analysis predicted modes one and three within an average of 23.1%, and modes two and four within an average of 4.4%.

14. SUBJECT TERMS
Finite Element Analysis, Piezoceramic, Modal Testing, Smart Structures

15. NUMBER OF PAGES
58

16. PRICE CODE

17. SECURITY CLASSIFICATION OF REPORT	18. SECURITY CLASSIFICATION OF THIS PAGE	19. SECURITY CLASSIFICATION OF ABSTRACT	20. LIMITATION OF ABSTRACT
Unclassified	Unclassified	Unclassified	UL

NSN 7540-01-280-5500

Standard Form 298 (Rev. 2-89)
Prescribed by ANSI Std. 239-18

Approved for public release; distribution is unlimited

FINITE ELEMENT ANALYSIS OF SMART STRUCTURES AND MODAL TESTING OF A FLEXIBLE SPACECRAFT ARM

by

James C. Trump
Commander, United States Navy
B.S, Civil Engineering, University of Notre Dame, 1976

Submitted in partial fulfillment
of the requirements for the degree of

MASTER OF SCIENCE IN ASTRONAUTICAL ENGINEERING

from the

NAVAL POSTGRADUATE SCHOOL
December 1994

Author: James C. Trump
James C. Trump

Approved by: B. N. Agrawal
Brij N. Agrawal, Thesis Advisor

Hyochoong Bang, Second Reader

Daniel J. Collins
Daniel J. Collins, Chairman
Department of Aeronautical/Astronautical Engineering

ABSTRACT

This thesis deals with analytical predictions and experimental determination of the modal frequencies and shapes associated with the arm portion of the Naval Postgraduate School's Flexible Spacecraft Simulator (FSS). A description of how piezoceramic sensors and actuators are incorporated in finite element modeling is presented. A MATLAB™ code conducting the finite element modeling of the arm is used to verify the modal frequencies generated via Structural Dynamic Research Corporation's I-DEAS™ software. Modal testing is conducted with the I-DEAS Test package to determine the first four physical modal frequencies and shapes so that we may compare them with the analytical results. The results of the testing indicated that finite element analysis predicted modes one and three within an average of 23.1%, and modes two and four within an average of 4.4%.

TABLE OF CONTENTS

I. INTRODUCTION

The often times prohibitive cost for putting payloads into orbit has lead the scientific and engineering community to design lightweight yet dynamically stable structures. Accurately predicting the natural frequencies of a structure, corresponding mode shapes and modal damping is integral to the design and dynamic control of such structures. Lightweight, flexible structures inherently possess low resonant frequencies which can easily be stimulated by a variety of spaceborne excitation sources such as attitude control thrusters and reaction wheels.

Previous work done on flexible structural control utilizing Positive Position Feedback (PPF) and Strain Rate Feedback (SRF) by Newman and Feuerstein, [Refs. 1 and 2] mandated an accurate knowledge of modal characteristics for successful control law design. This previous work in modal control provides the stimulation for this research.

The most common method of modal frequency and shape prediction is some form of the Finite Element Analysis (FEA) approach. This method exploits digital computing power and provides a formulation for the analysis of dynamic characteristics of flexible structures. By regarding a complex structure as a composite of finite elements, the method requires that displacements be compatible and internal forces in equilibrium at points known as nodes, which are shared by several elements. The result being the total structure should act as if one continuous entity.

The Naval Postgraduate School Flexible Spacecraft Simulator's arm provides a testbed for modal analysis. It provides a reasonably accurate representation of a very flexible arm such as that which might be utilized for a deployed antenna, possibly imposing very accurate pointing constraints. This arm employs nearly collocated piezoceramic actuators and sensors for the damping and control of vibration. The FEA method is well documented, [Refs. 3 and 4]. What is initially explored is how the physical properties and

forces implied to a structure via the incorporation of these piezoceramic sensors and actuators modifies the FEA.

Many commercial software FEA packages are available to assist with the predictions described above. For the purpose of this thesis, the modal prediction package provided by Structural Dynamic Research Corporation's I-DEAS software is used. A comparison of this output to a simple MATLAB code which utilizes standard FEA techniques [Ref. 4] is then undertaken.

Finally, modal analysis of the arm is conducted experimentally so that we may determine the accuracy of analytical predictions. This modal testing utilizes the testing package incorporated within the I-DEAS software. The arm is excited at several nodes with an impact hammer with a built-in force transducer. Accelerations of the arm are measured via an accelerometer whose signal has been conditioned and amplified. These analog time domain signals are discretized and then changed into the frequency domain via the discrete Fourier transform. The analyzed signals can then be manipulated in a variety of ways to produce such information as natural frequencies, mode shapes and damping ratios.

II. FINITE ELEMENT ANALYSIS WITH PIEZOCERAMIC ACTUATORS AND SENSORS

A. ANALYTICAL BACKGROUND AND ASSUMPTIONS

For the purpose of discussing the procedure with which FEA methods are modified to take into effect the physical and active characteristics of an element incorporating piezoceramics, consider the co-located sensor/actuator pair on the **n**-th element of an isotropic flexible beam as depicted in Figure 1 below. All physical and electrical properties and dimensions of the actuator and sensor are assumed identical. The neutral axis is aligned with the centerline of the beam. The beam is free to translate in the +/- number 3 axis direction and rotate about the number 2 axis only.

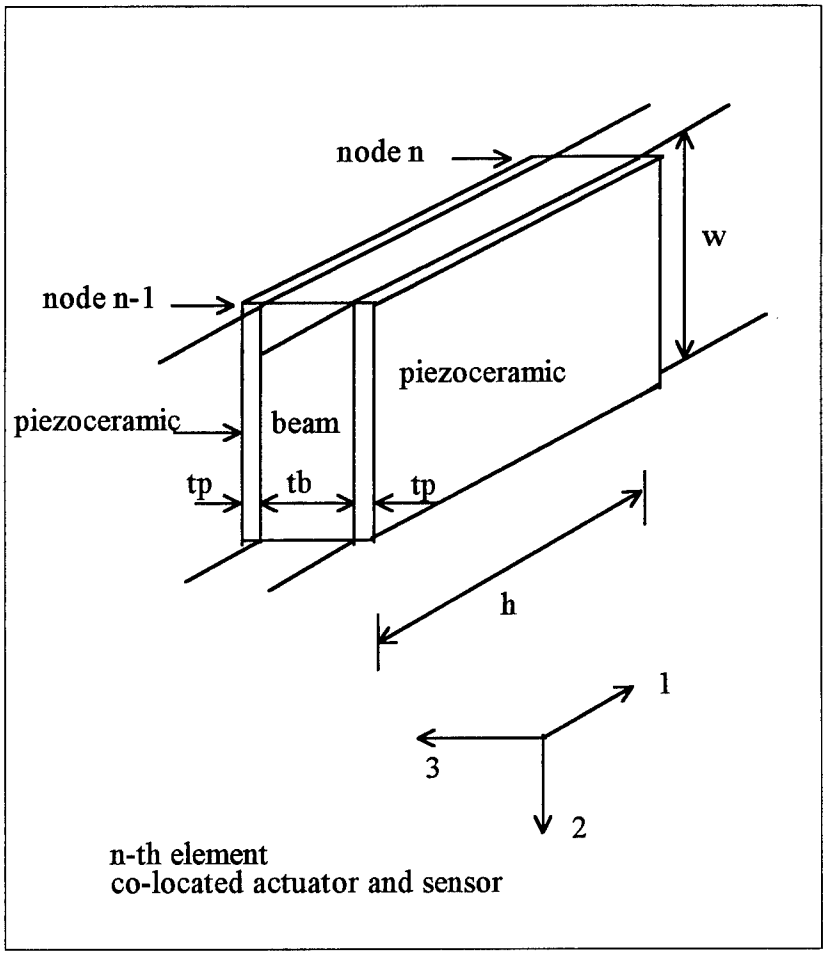

Figure 1. Piezoceramic Actuator and Sensor, **n**-th Element

B. GOVERNING EQUATIONS

1. Passive Contributions

We first consider a structural element as shown in Figure 2. The equations of motion for the element are of the form:

$$M\ddot{q} + Kq = 0 \tag{1}$$

where M and K are the elemental mass and stiffness matrices, respectively. q represents an element displacement vector of the form:

$$q = \begin{Bmatrix} w_{n-1} \\ \theta_{n-1} \\ w_n \\ \theta_n \end{Bmatrix} \tag{2}$$

where w_{n-1} and w_n are the transverse deflections of the left and right end of element **n**, respectively, and θ_{n-1} and θ_n are the rotations of the left and right end of element **n**, respectively. These displacements are shown in Figure 2 below.

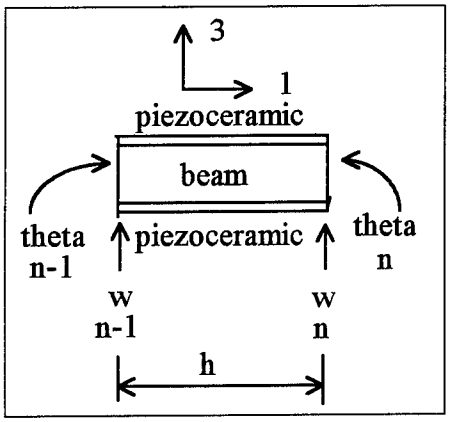

Figure 2. **n**-th Element Displacements

By deriving the equations of motion for the element using Lagrange's equations, which reduces, in turn, to determining the kinetic energy, the potential energy, and the virtual work expressions in terms of the nodal cordinates, consistent element mass and stiffness matrices can be generated.

The consistent element mass and stiffness matrices are given by the following:

$$M = \frac{mh}{420}\begin{bmatrix} 156 & 22h & 54 & -13h \\ 22h & 4h^2 & 13h & -3h^2 \\ 54 & 13h & 156 & -22h \\ -13h & -3h^2 & -22h & 4h^2 \end{bmatrix} \quad (3)$$

$$K = \frac{EI}{h^3}\begin{bmatrix} 12 & 6h & -12 & 6h \\ 6h & 4h^2 & -6h & 2h^2 \\ -12 & -6h & 12 & -6h \\ 6h & 2h^2 & -6h & 4h^2 \end{bmatrix} \quad (4)$$

where m is the linear mass density of the element, h is element length, E is Young's modulus for the element and I is the element moment of inertia about the bending axis. [Ref. 4]

In order to account for piezo contribution to the mass matrix, m must be equal to the linear mass density of the beam plus the linear mass density of the piezoceramic actuator and sensor, or,

$$m = m_{beam} + m_{piezo} \quad (5)$$

To account for piezo contribution to the stiffness matrix, the EI term must be of the form:

$$EI = E_{beam}I_{beam} + E_{piezo}I_{piezo} \quad (6)$$

Since the neutral axis is aligned with the beam centerline, I_{beam} is simply:

$$I_{beam} = \frac{wt_b^3}{12} \quad \text{(about bending axis)} \quad (7)$$

where w is the width of the element and t_b is the thickness of the structure.

By employing the parallel axis theorem to determine I_{piezo}, we arrive at the following:

$$I_{piezo} = 2[\frac{wt_p^3}{12} + (wt_p)(\frac{t_b}{2} + \frac{t_p}{2})^2] \quad (8)$$

where t_p is the thickness of the piezoceramic.

After simplification,

$$I_{piezo} = 2wt_p\left(\frac{t_b^2}{4} + \frac{t_p t_b}{2} + \frac{t_p^2}{3}\right) \quad (9)$$

E_{beam} and E_{piezo} are simply the Young's modulus values for the beam and piezo, respectively.

Once the particular elements incorporating the piezos are modified as above, all other aspects of constructing the global mass and stiffness matrix for an entire structure incorporating multiple elements are straightforward [Ref. 4]. The global version of Equation (1) will now present an eigenvalue problem whose solution will reveal modal frequencies and shapes.

2. Active Contributions

a. *Sensor*

Piezoceramic actuator and sensor theory is well documented [Ref. 5]. Voltage output from the piezoceramic sensor is given by the following equation:

$$V_s = t_p(E_p d_{31}/D)(\varepsilon_1 + \varepsilon_2) \tag{10}$$

where

t_p is the thickness of the piezoceramic sensor
E_p is Young's modulus for the sensor in N/m^2
d_{31} is the lateral strain coefficient in m/V or Coul/N
D is Abs Permittivity in Farad/m or N/V^2
ε_1 and ε_2 are longitudinal and lateral strain, respectively

Since longitudinal strain ε_1 and the lateral strain ε_2 are related by Poison's ratio, ν, given by:

$$\varepsilon_1 \nu = -\varepsilon_2 \tag{11}$$

Equation (10) may be written as:

$$V_s = t_p(E_p d_{31}/D)(1 - \nu)\varepsilon_1 \tag{12}$$

Figure 3 illustrates the sensor mode of the piezoceramic. The illustration on the left of Figure 3 depicts the case when the sensor is subject to lateral tension and vertical compression. The right illustration shows the sensor in vertical tension and lateral compression. Produced voltage polarities under these conditions for the indicated poling direction are as shown.

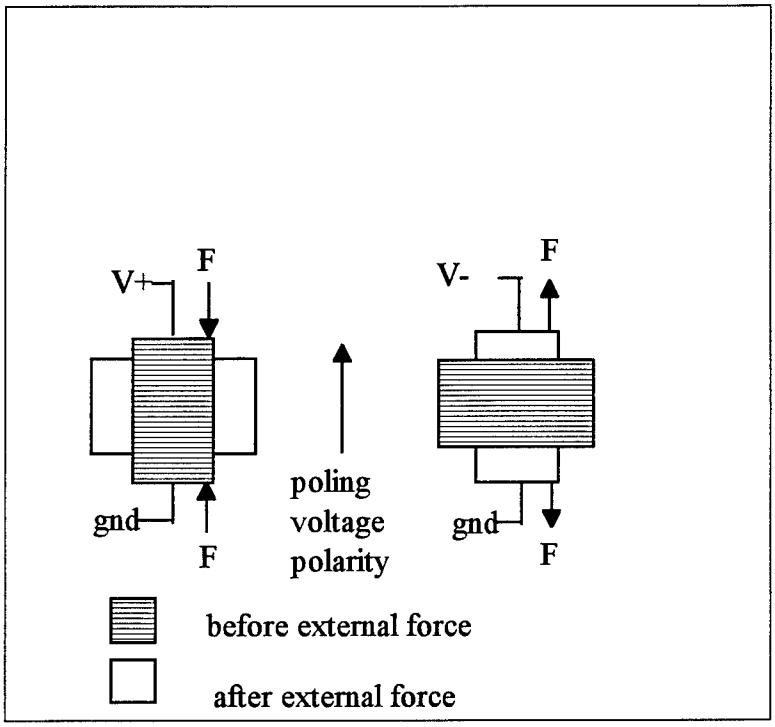

Figure 3. Piezoceramic Sensor

In generalized coordinates, sensor voltage produced at the **n**-th element is represented by the following, [Ref. 5]:

$$V_s' = V_s\begin{bmatrix} 0 & 1 & 0 & 1 \end{bmatrix}q \tag{13}$$

where V_s is given by Equation **(12)** and the displacement vector q, is given by equation **(2).**

b. ***Actuator***

The equation with which the general behavior of the element, exposed to external excitation forces and also the forces imposed by the actuator, is represented by the following:

$$M\ddot{q} + Kq = F_{external} + F_{actuator} \tag{14}$$

where $F_{actuator}$ is given by the following expression, [Ref. 5]:

$$F_{actuator} = -BV_a \tag{15}$$

V_a is the voltage applied to the actuator and B is a 4 x 1 vector possessing moment correction terms whose units are in Newton- meters/volt:

$$B = \begin{Bmatrix} 0 \\ b_2 \\ 0 \\ b_4 \end{Bmatrix} \tag{16}$$

with

$$b_2 = -d_{31}E_p w(\tfrac{t_b}{2} + \tfrac{t_p}{2}) \qquad \text{and} \qquad b_4 = -b_2 \tag{17}$$

where all variables are as in Equation **(10)** and w is the actuator width. Figure 4 illustrates the actuator mode of the piezoceramic. The left side illustration demonstrates vertical contraction and the corrective moment producing lateral expansion when applied voltage is of opposite polarity from the poling voltage. The right side demonstrates vertical expansion and the corrective moment producing lateral contraction when a voltage of the same polarity as the poling voltage is applied to the piezo.

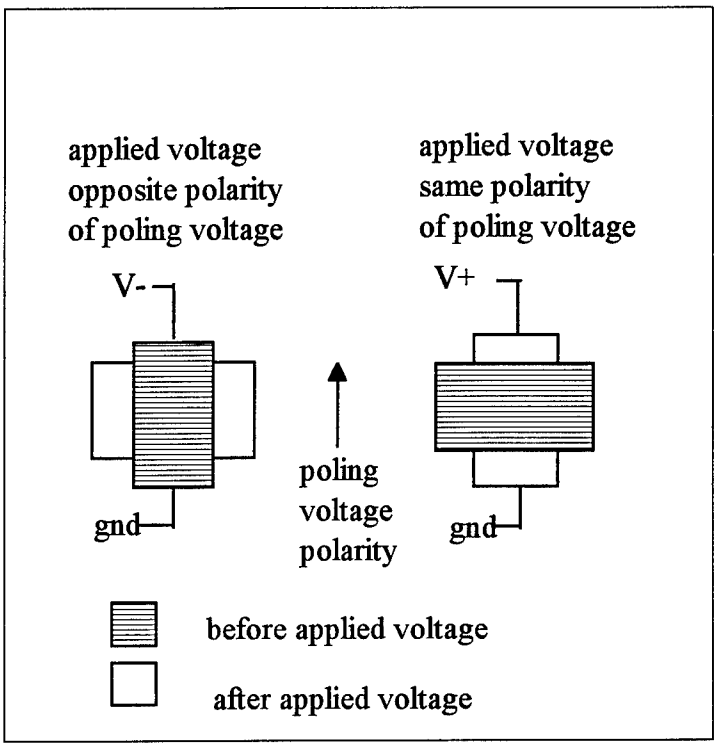

Figure 4. Piezoceramic Actuator

c. *Coupling Sensor Output to Actuator Input*

The last procedure is to determine the control scheme which will couple the measured sensor voltage output to that applied to the actuator in order to produce a restoring moment to the element and ultimately the entire structure itself. We will examine a simple implementation of velocity feedback, where

$$V_a = k\dot{V}_s' \tag{18}$$

k is a voltage gain factor. Combining all variables in Equations **(2)**, **(13)** and **(15)** will ultimately lead to the following overall expression for $F_{actuator}$:

$$F_{actuator} = -k\begin{Bmatrix} 0 \\ b_2 \\ 0 \\ b_4 \end{Bmatrix} V_s \begin{bmatrix} 0 & 1 & 0 & 1 \end{bmatrix} \begin{Bmatrix} \dot{w}_{n-1} \\ \dot{\theta}_{n-1} \\ \dot{w}_n \\ \dot{\theta}_n \end{Bmatrix} \tag{19}$$

With the variables b_2 , b_4 and V_s as before. Equation **(19)** can now be written in the form:

$$F_{actuator} = -C\dot{q} \tag{20}$$

where C is a 4 x 4 matrix given by:

$$C = -k\begin{Bmatrix} 0 \\ b_2 \\ 0 \\ b_4 \end{Bmatrix} V_s \begin{bmatrix} 0 & 1 & 0 & 1 \end{bmatrix} \tag{21}$$

With no external excitation forces present, Equation **(14)** may now be rewritten in the general damped form:

$$M\ddot{q} + C\dot{q} + Kq = 0 \tag{22}$$

In the construction of a global system of i number of elements, the global C matrix will be null in all segments except those which possess actuators. Therefore, the passive damping of the structure is neglected. Equation **(22)** then presents a conventional eigenvalue problem which will reveal modal frequencies, modal vectors and damping ratios. [Ref. 6]

III. FINITE ELEMENT ANALYSIS COMPUTER PREDICTIONS

A. I-DEAS™ FEA MODELING

I-DEAS is a menu driven, Windows™ type, software package developed by Structural Data Research Corporation. Its finite element analysis and testing packages are just two of several structural design tools available to designers and engineers.

The first step in conducting FEA with I-DEAS is to model the structure under consideration. Figure 5 depicts the mesh geometry for the Flexible Spacecraft Simulator's arm used for the analysis. This flexible arm rests on a granite table which simulates a friction free environment and is supported at the elbow and tip by two airpads (nodes 10 and 19). Node 1 is rigidly fixed to the table. Mesh geometry is such that the arm is free to translate in the +/- number 1 and 3 axis and rotate about the number 2 axis only.

The arm is constructed of 7075 T-6 aluminum, with a cross section of 1/16" x 1" (t_b x w), and has several mass intensifiers, which are treated as point masses for the purpose of the analysis, spaced throughout the beam. Elements 1, 10, 11, and 18 have two wafers per side of Navy Type II PZT bonded to the beam surface. Table 1 below cites the material and electrical properties of this piezoceramic.

Quantity	Description	Units	Value
d_{31}	Lateral strain coeff	*m/V or Coul/N*	1.8 e-10
E_{piezo}	Young's modulus	*Pascal*	6.3 e10
ν	Poison's ratio	n/a	0.35
D	Abs Permittivity	*Farad/m or* N/V^2	1.5 e-8
t_p	piezo thickness	m	1.905 e-4
ρ_{piezo}	Mass density	kg/m^3	7.7 e 3

Table 1. Navy Type II PZT Properties

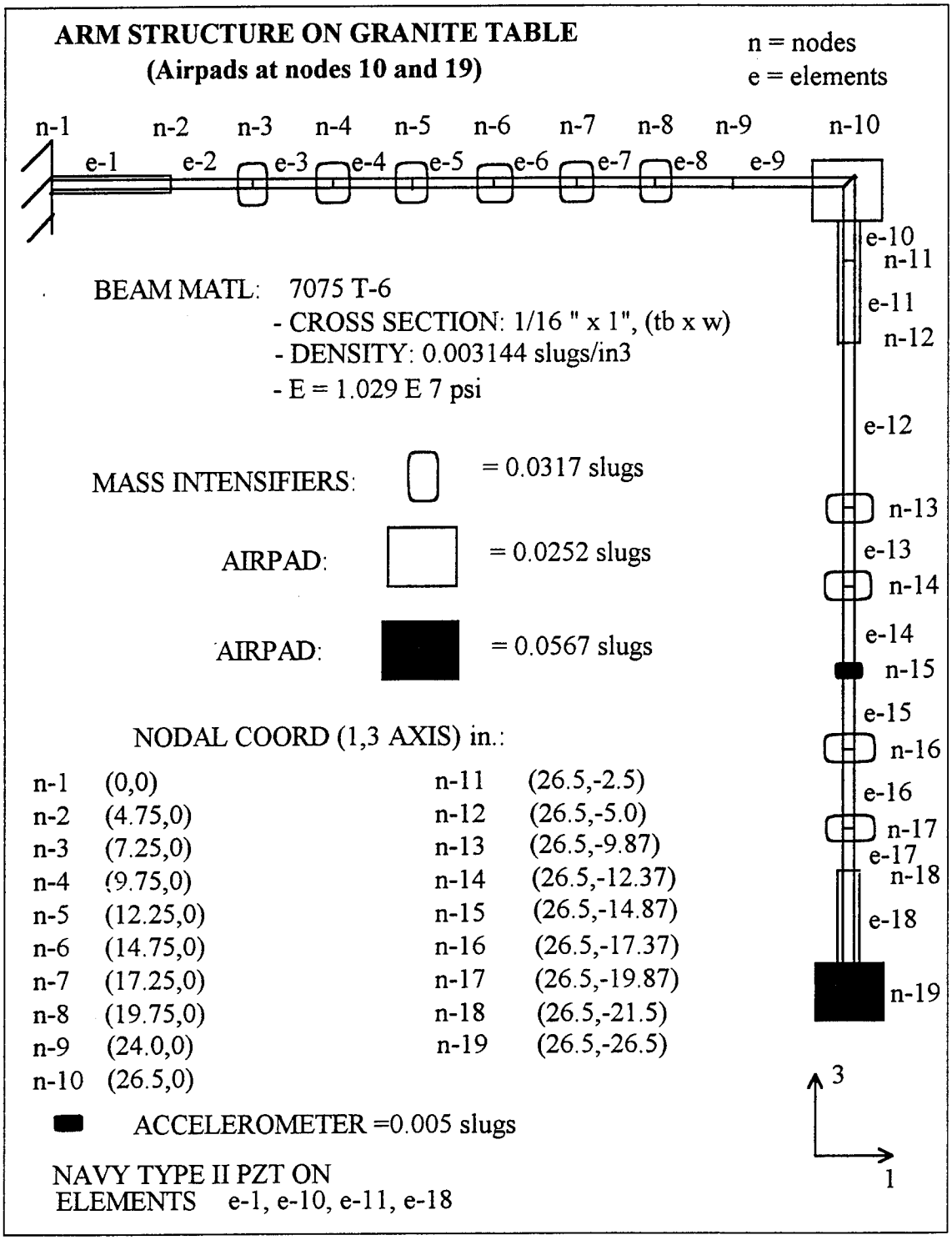

Figure 5. Finite Element Analysis Mesh for

Flexible Spacecraft Simulator Arm

The mesh geometry (all nodal coordinates), beam element geometry, element material properties, point mass locations and values, and structural restraints are all input into the I-DEAS modeler. Once this model is stored, modal analysis can be conducted. I-DEAS constructs element mass and stiffness matrices, assembles the global mass and stiffness matrices for the structure and then calculates the modal frequencies and associated mode shapes. Modal analysis was conducted on models with and without the PZT wafers on elements 1, 10, 11, and 18. **Appendix A** contains the I-DEAS printouts for the model, and the deformed geometry for the first four modes, with and without piezoceramic contribution on elements 1, 10, 11, and 18. Table 2 below lists the frequencies associated with the first four modes generated by I-DEAS FEA for the arm.

Mode	Frequency (Hz) (without piezos)	Frequency (Hz) (with piezos)
1	0.136	0.159
2	0.372	0.469
3	1.651	1.87
4	2.373	3.06

Table 2. I-DEAS FEA Modal Frequencies

B. MATLAB™ FEA MODELING

The MATLAB code used to conduct FEA on the FSS arm appears in **Appendix B.** No control laws were implemented relating sensor output to actuator input. The code, therefore, performs the eigenvalue problem shown in Equation **(2).** This code was also run with and without the PZT properties included in order to compare it with the I-DEAS output. **Appendix C** contains printouts of the modal frequencies, with and without piezos, in descending order. Table 3 below lists the modal frequency predictions, for the first four modes, generated from MATLAB. The I-DEAS predictions are also re-listed for comparisons sake.

Mode	MATLAB (with piezos) (Hz)	I-DEAS (with piezos) (Hz)	MATLAB (without piezos) (Hz)	I-DEAS (without piezos) (Hz)
1	0.162	0.159	0.136	0.136
2	0.46	0.469	0.373	0.372
3	1.787	1.87	1.646	1.651
4	2.851	3.06	2.373	2.373

Table 3. MATLAB and I-DEAS FEA Modal Frequencies

As seen from the table, MATLAB and I-DEAS modal frequency predictions for both cases correlate well. For the case with piezo contribution to the arm considered, the I-DEAS predictions diverge slightly from MATLAB. The MATLAB and I-DEAS predictions for the arm without piezo contribution considered are essentially the same. The overall effect of the piezos on the arm stiffens the structure incrementally, as evidenced by the slightly higher frequencies generated by both MATLAB and I-DEAS.

IV. MODAL TESTING

A. INTRODUCTION

In Chapters II and III, the differential equations, or models, of the system are assumed to be known, and the theory developed consists of calculating and characterizing the response of the system to known inputs. This is called the "forward problem". In this chapter the interest lies in measuring the response of a structure and in some way determining the equations of motion from the test data. The problem of determining a system of equations from information about inputs and responses belongs to a class of problems called "inverse problems", or system identification. The measurement of the vibrational behavior of the structure is used to verify the mathematical model of the test structure outlined in Chapters II and III. [Ref. 3]

Modal testing is the interpretation of test data collected from a vibrating structure. The purpose of a modal test is to construct a mathematical model of the vibrational properties and dynamic behavior of the tested structure.

Modal testing focuses on frequency, shape determination and damping. On a plot of frequency response as a function of frequency, a resonance frequency (modal frequency) is marked by a peak of the magnitude. A second phenomena of resonance is that the phase of the response shifts by 180 degrees as the frequency sweeps through resonance, with the value of the phase at resonance being 90 degrees.

B. MEASUREMENT HARDWARE

Vibration measurement generally requires several hardware components. These consist of a source of excitation for providing a known and controlled input to the structure, a transducer or accelerometer which converts mechanical motion of the structure to an electrical signal, and a signal conditioning amplifier to match the signal level of the accelerometer to that of the data acquisition system. This data acquisition system provides the interface between excitation forces and accelerometer signals to the testing software imbedded within I-DEAS.

Appendix D delineates all hardware associated with modal testing of the FSS arm. An impact hammer with a built-in force transducer was used to excite the structure. Although the impact hammer is simple and adds no mass to the arm, it sometimes may be incapable of transforming sufficient energy to the structure to develop adequate response signals in the frequency range of interest. Consistent impact techniques can also be difficult to develop. The key frequency range of interest for this test was from 0 to 4 Hz. This bandwidth would hopefully contain resonance information for the first four flexible modes.

C. DIGITAL SIGNAL PROCESSING

Modal Testing analysis is performed in the frequency domain. The data acquisition system converts the analog time domain signals into the digital frequency domain via the Discrete Fourier transform. This data is then passed on to I-DEAS in order to perform the required computations. Briefly, by comparing the transfer functions of the response of the structure to the transfer function of the excitation force, one can determine the transfer function of the structure itself and ultimately its associated resonances. Mode shapes may also be extracted from this data. The transfer function relationship is given by:

$$G(j\omega) = S_{fx}(j\omega)/S_{ff}(j\omega) \tag{23}$$

where,

$S_{fx}(j\omega)$= response of the structure in the frequency domain, ω

$S_{ff}(j\omega)$= excitation force in the frequency domain, ω

$G(j\omega)$= the transfer function of the structure

Reference 7 provides an excellent source for information on the theoretical and practical problems surrounding the measurement, processing, and analysis of modal test data.

D. TEST PROCEDURES

A modal test mesh must be created within the I-DEAS testing environment. This mesh is depicted in Figure 6. Unlike the mesh created for the finite element analysis, no material properties need be entered. The nodal coordinates in this mesh defines the degrees of freedom for the structure. The accelerometer was located at nodes 13, 10 and 8 for the bulk of the testing due to physical constraints (proximity to the piezos and associated wiring). Node 16 was used as the primary impact location for defining the first four modal frequencies. Impact at this location proved to consistently and reliably excite the first four modal frequencies. Impact at all other nodes was performed in order to determine mode shapes. [Ref. 8]

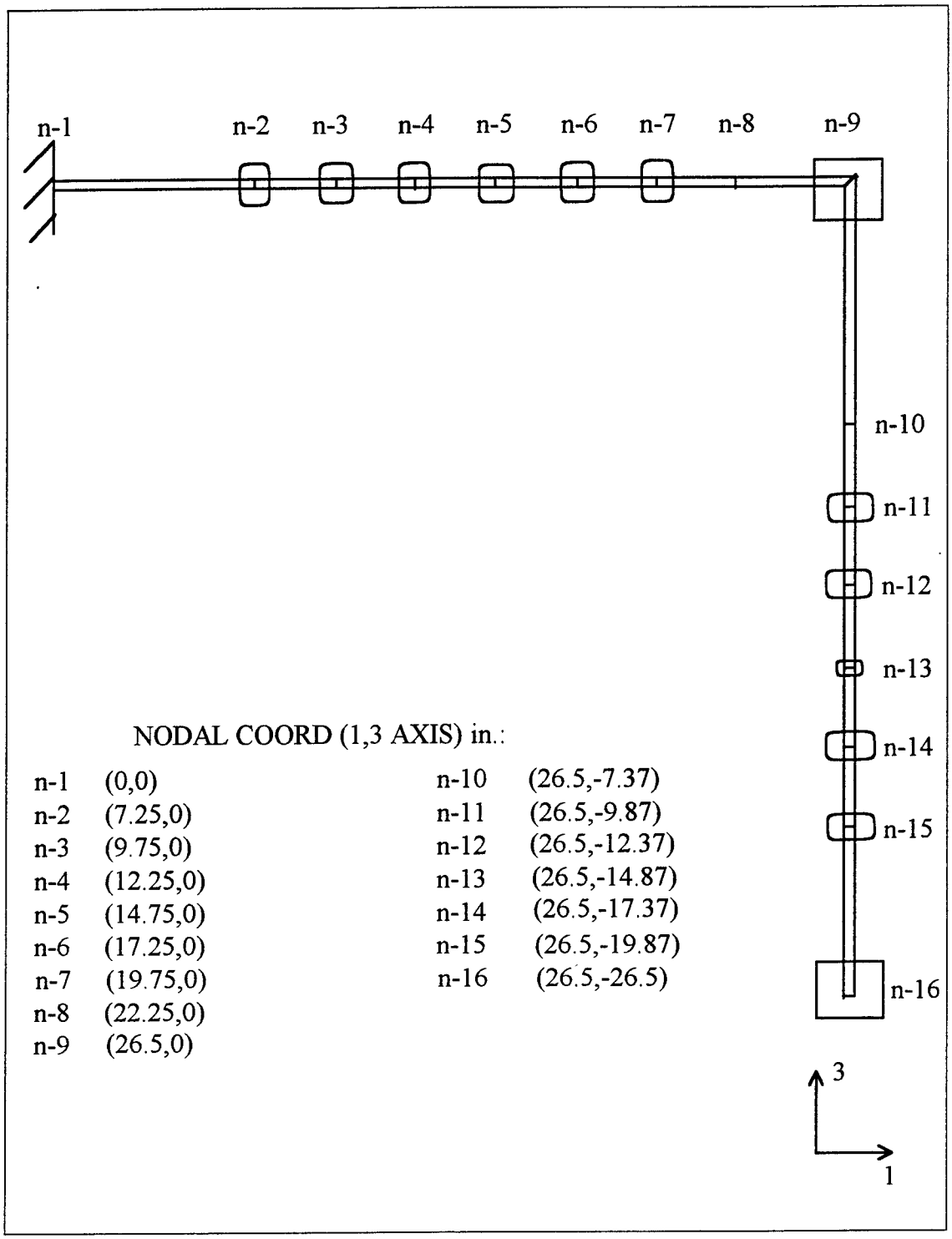

Figure 6. Modal Test Mesh for

Flexible Spacecraft Simulator Arm

E. TEST RESULTS

Figures 7, 8 and 9 are I-DEAS printouts of the arm's frequency response function measured at nodes 13, 10 and 8 respectively. Impact for all three of these measurements took place at node 16. The resonant frequencies are clearly represented by distinct peaks. The 180 degree phase shift (or phase reversal) crossing resonance is also reasonably well defined. Table 4 below lists the averages of the modal frequencies observed during these tests at nodes 13, 10 and 8. The table also re-lists the MATLAB FEA predictions (with piezoceramic contribution) and a percent deviation.

Mode	Modal Test Frequency Averages (impact at node 16, response at nodes 13, 10 and 8) (Hz)	MATLAB FEA Prediction (with piezos) (Hz)	% Deviation
1	0.124	0.162	23.4
2	0.436	0.46	5.2
3	1.374	1.787	22.8
4	2.751	2.851	3.5

Table 4. Modal Test Averages and % Deviation from FEA

Figure 10 depicts an analytical curvefit that was performed by I-DEAS on the test data obtained at node 13. This analytical curve is distinguished from the raw data by its smooth character. The peaks identified by this curvefit are essentially identical to those shown on Figure 7. The frequency data extracted from this curvefit was input to the mode shape subroutine within the I-DEAS Testing package.

Figure 11 compares the third mode shape generated by I-DEAS FEA to that actually observed during modal testing. The bottom illustration of Figure 11 is the third

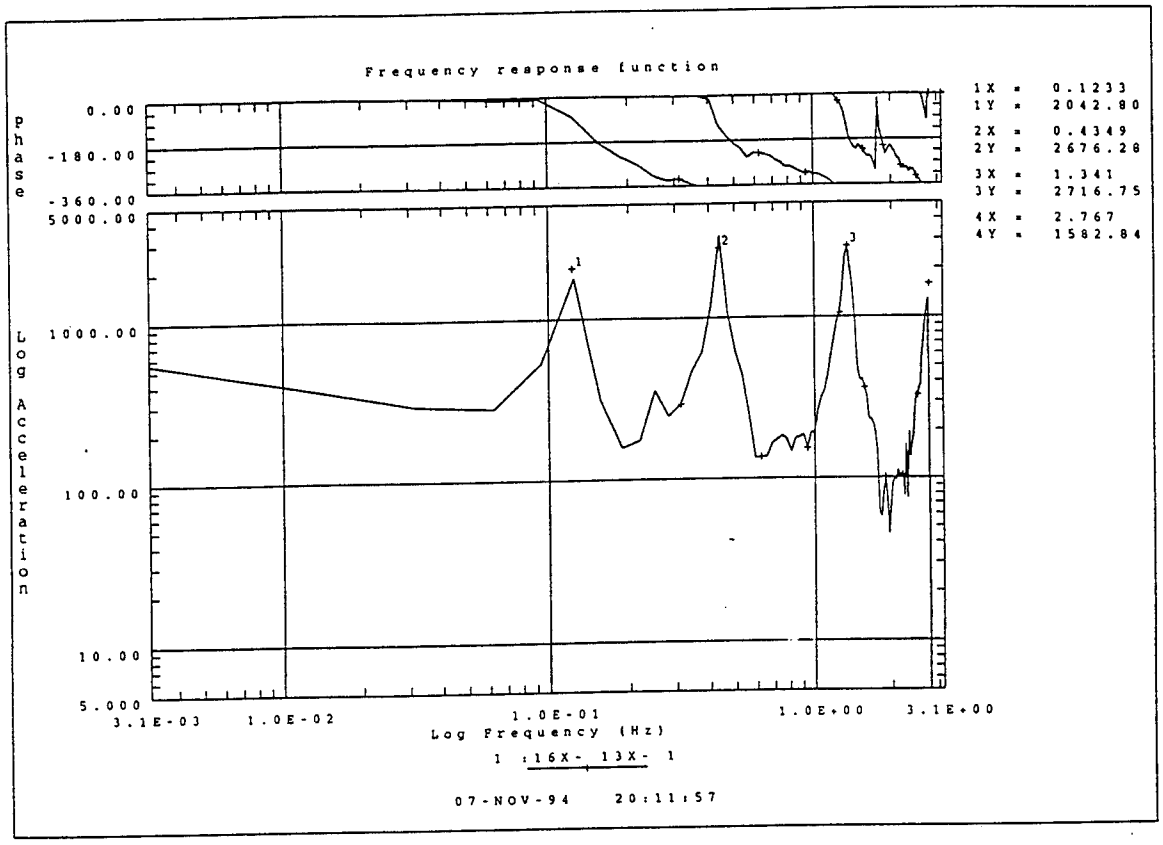

Figure 7. Modal Test Response Function (impact at node 16, accelerometer at node 13)

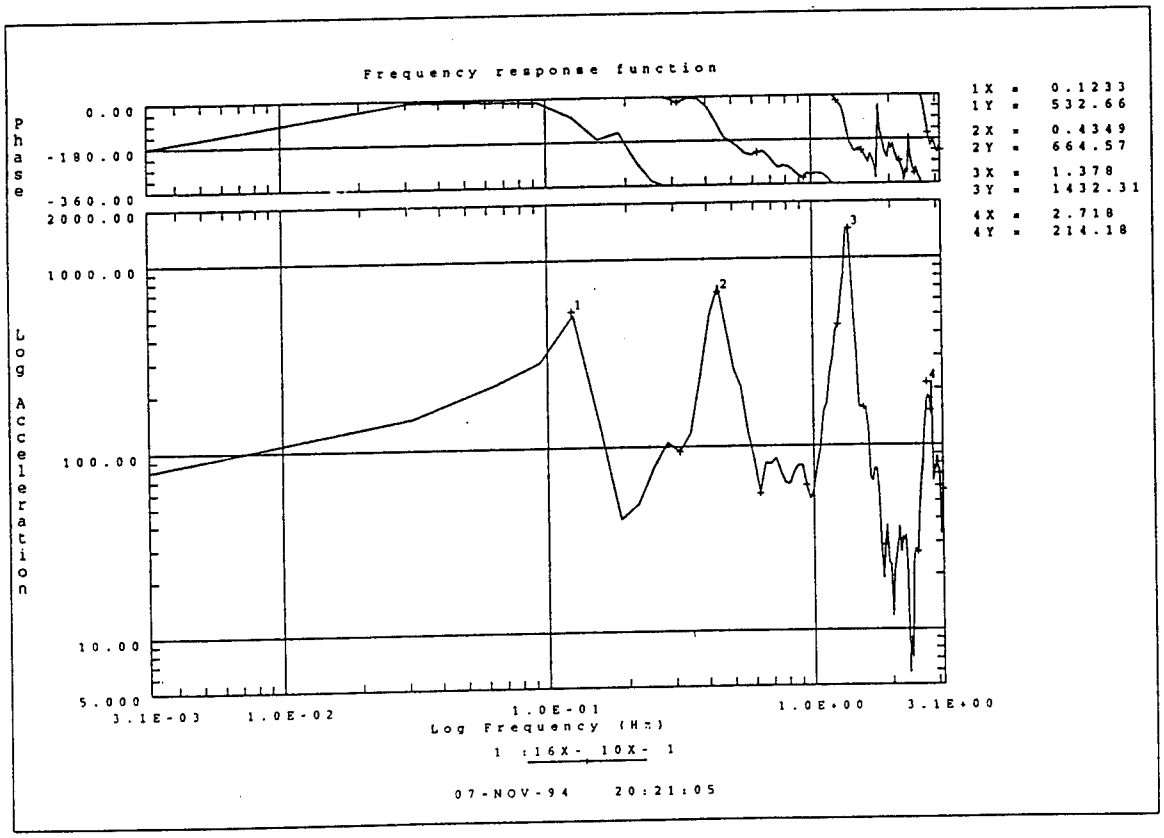

Figure 8. Modal Test Response Function (impact at node 16, accelerometer at node 10)

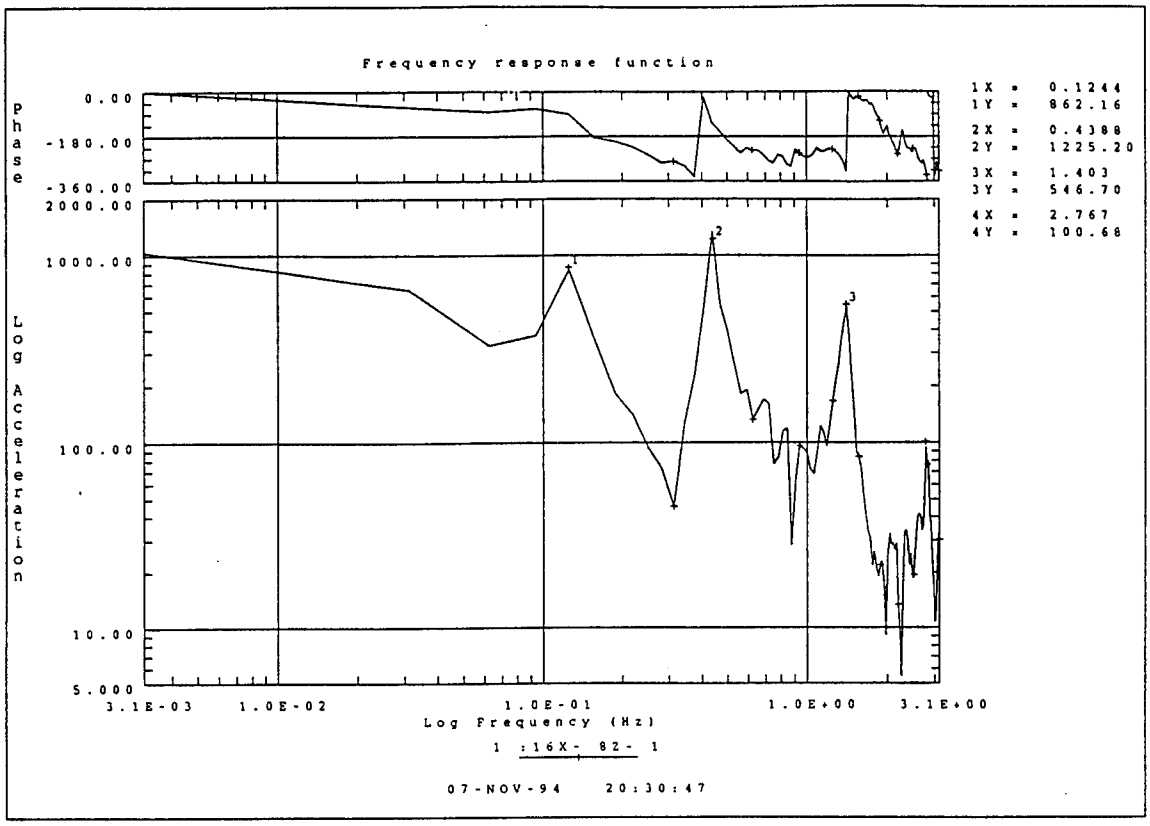

Figure 9. Modal Test Response Function (impact at node 16, accelerometer at node 8)

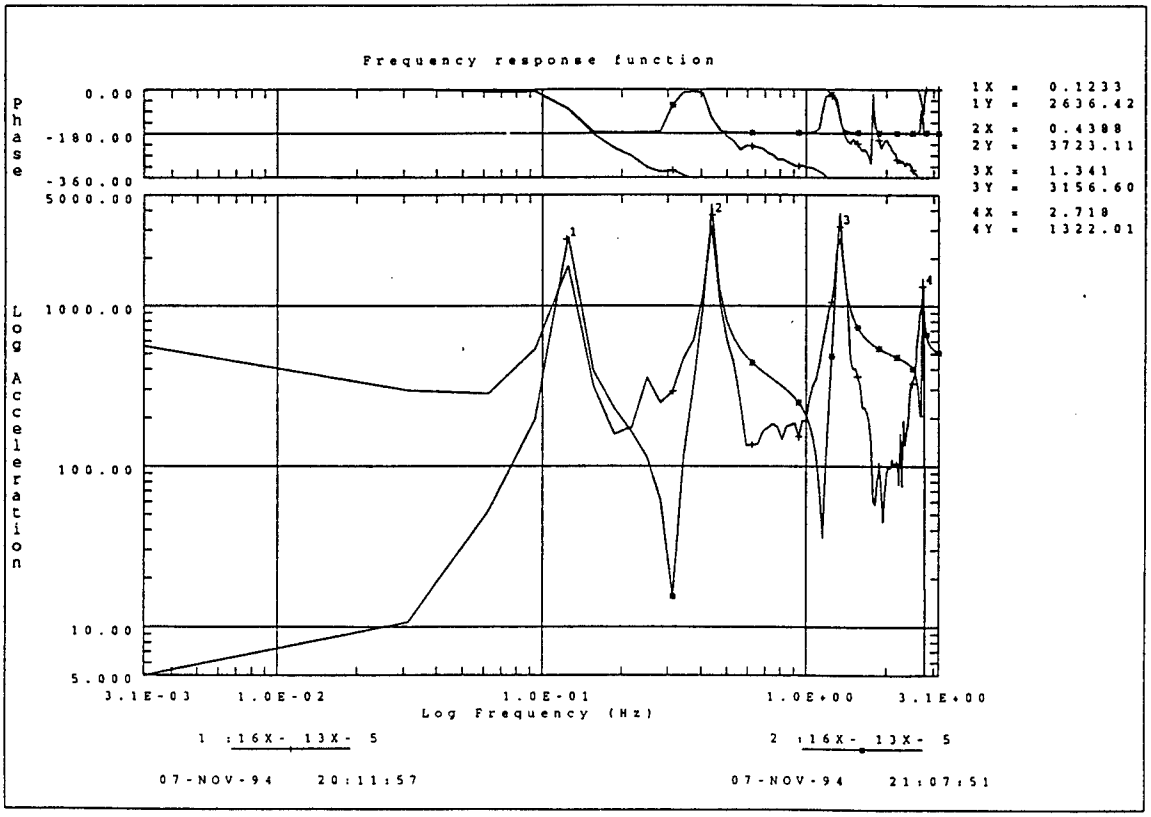

Figure 10. Modal Test Response Function Analytical Curvefit
(impact at node 16, accelerometer at node 13)

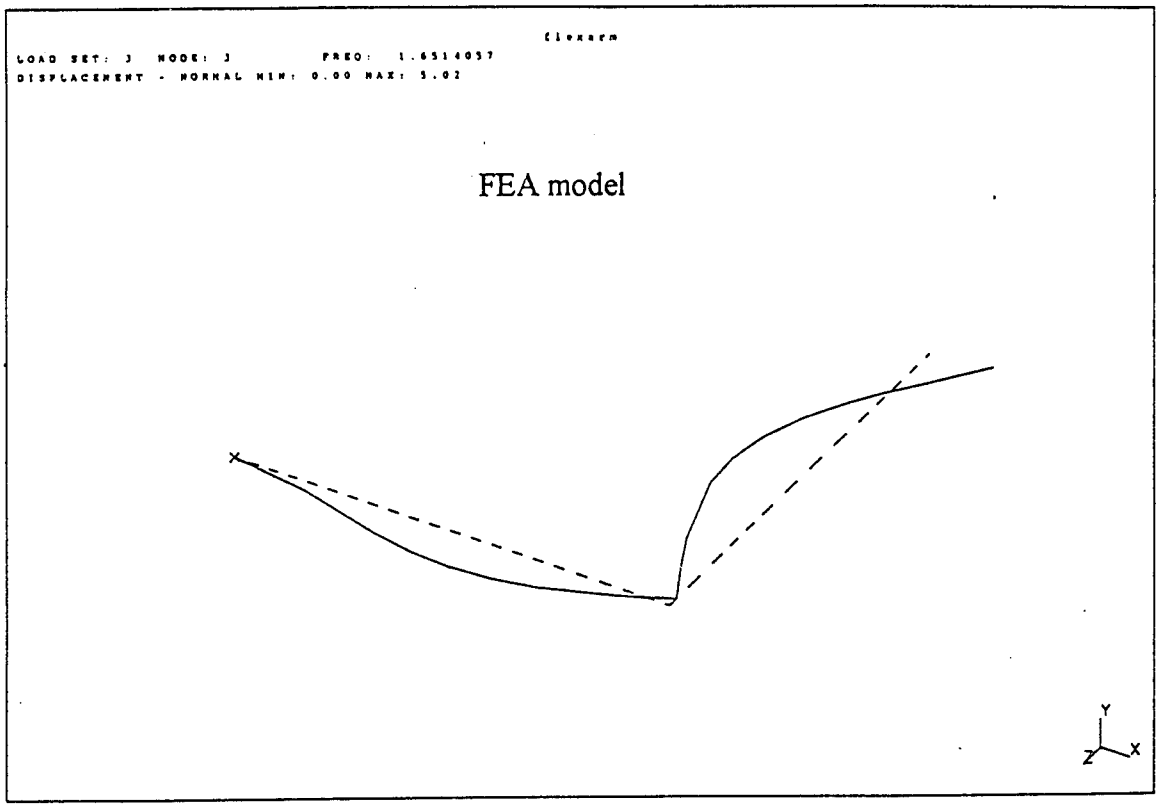

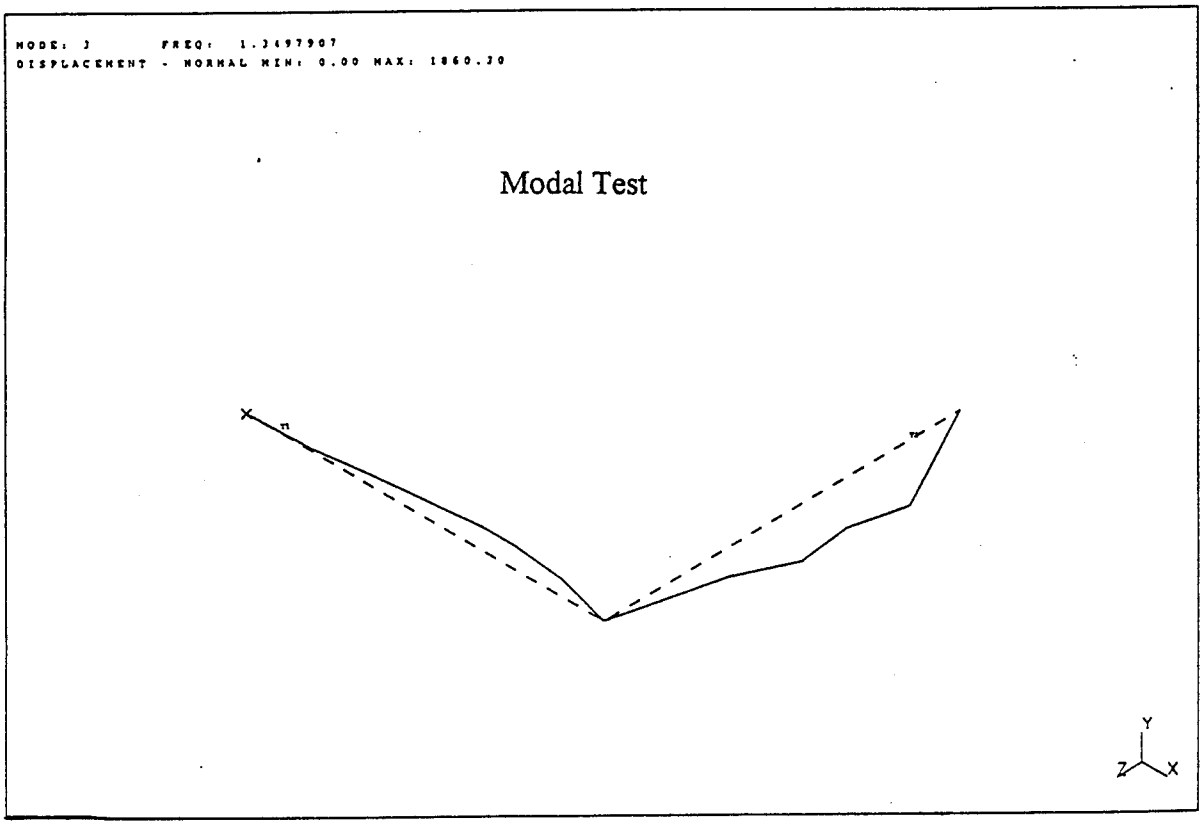

Figure 11. Mode 3 Shape (FEA and Modal Test)

mode shape generated during the testing, the top represents the prediction of mode 3 behavior via FEA.

A structure's inherent damping characteristics can only be determined experimentally. An **n** degree of freedom system has **n** damping ratios, ζ_i, (dimensionless) one associated with each modal frequency, ω_i, (radians per second). The free vibration characteristics of each mode decays over time, t, according to the term:

$$e^{-\zeta_i \omega_i t} \tag{23}$$

[Ref. 9]. Table 5 lists the damping ratios for the first through fourth modes obtained from the I-DEAS testing package. The exponential time decay coefficient is also listed.

Mode, i	ζ_i	$\omega_i = 2\pi(freq)$ (radians/s)	$\zeta_i \omega_i$
1	0.026	0.779	0.02
2	0.018	2.739	0.049
3	0.013	8.633	0.112
4	0.005	17.285	0.086

Table 5. Modal Test Damping Ratios

V. CONCLUSIONS AND RECOMMENDATIONS

The major reason for conducting model testing is for comparison and verification of analytical models. What is ultimately desired is a mathematical model of the structure under consideration for the purpose of predicting how the structure will behave under a variety of different loadings, to provide the plant in a control system design, such as Positive Position Feedback (PPF) or Strain Rate Feedback (SRF), and to aid in the design process in general.

Modal testing of the FSS arm provided valuable insight into this field. Testing results yielded resonant frequencies that deviated from prediction by as little as 3.5% for mode four, and as much as 23.4% for mode one. Overall, modes one and three deviated from prediction on the average of 23.1%, and modes two and four deviated on the average of 4.4%. The difference between the analytical prediction and experimental determination of frequency for the first mode is significant. Further work is required to improve the model and/or improve the modal testing technique.

The damping ratios obtained during modal testing are that of an underdamped system, $(\zeta_i < 1)$, [Refs 3 and 4]. The expected dominance of mode one is supported by the lowest exponential time decay coefficient.

As mentioned earlier, the most common application of modal testing is the comparison of measured vibration modes with those predicted by a finite element or other theoretical models. Resonance frequencies must be accurately identified, also a complete and accurate description of mode shapes is desired, especially for non-collocated sensor and actuator systems. Frequently, the analytical model will not predict the measured frequencies. As a result the analytical model may then be updated, iteratively, until it produces the measured natural frequencies. The modified model is then considered an improvement over the previous model. [Ref. 3]

One possible model modification would be to consider the inertial contributions of the mass intensifiers and airpads. These were treated as point masses with zero moment of inertia. This would be a good starting point in model evolvement.

Normally, the FSS arm is attached to the center body of the FSS which houses the reaction wheel and thrusters [Ref. 2]. With at least two additional "zero-Hz operation" accelerometers, such as that used for this experiment, placed on the arm (total of three on the arm), and with an additional and suitable accelerometer mounted to the center body for excitation source measurement, more reliable frequency measurements may be expected. These results may then be used to "tweak" any implementation of PPF or SRF that may be used for active control, in more of a real time fashion.

APPENDIX A

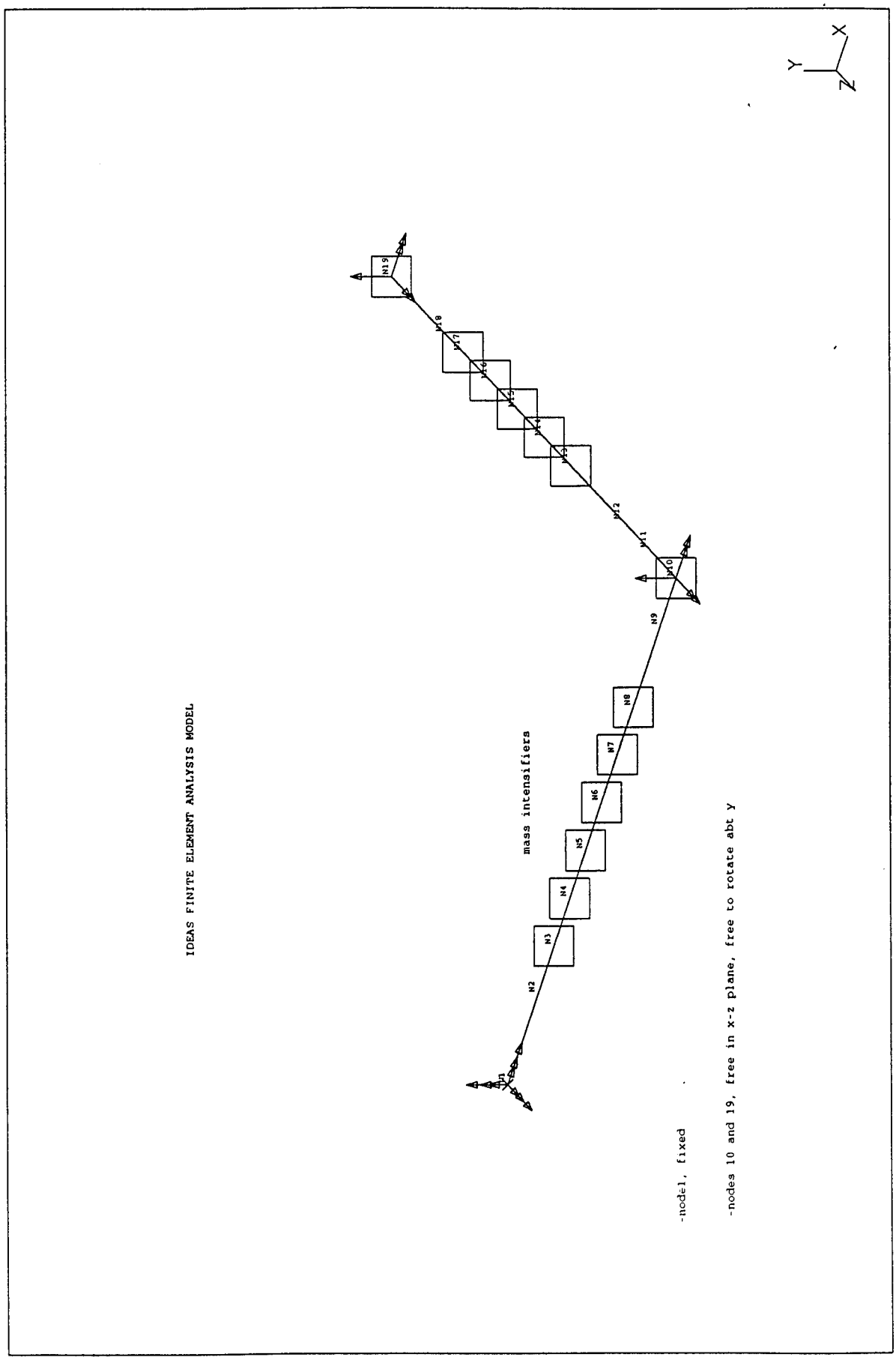
IDEAS FINITE ELEMENT ANALYSIS MODEL
mass intensifiers
-node1, fixed
-nodes 10 and 19, free in x-z plane, free to rotate abt y
X
Y
Z
N1
N2
N3
N4
N5
N6
N7
N8
N9
N10
N11
N12
N13
N14
N15
N16
N17
N18
N19

flexarm

LOAD SET: 1 MODE: 1 FREQ: 0.13591756

DISPLACEMENT - NORMAL MIN: 0.00 MAX: 27.53

without piezos

IDEAS FINITE ELEMENT ANALYSIS MODEL

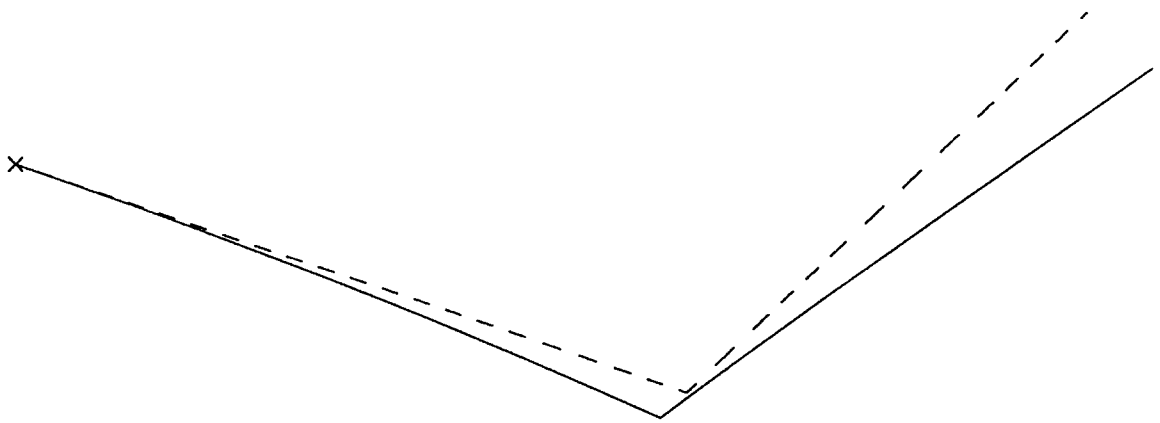

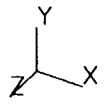

flexarm

LOAD SET: 2 MODE: 2 FREQ: 0.37213859
DISPLACEMENT - NORMAL MIN: 0.00 MAX: 22.19

without piezos

IDEAS FINITE ELEMENT ANALYSIS MODEL

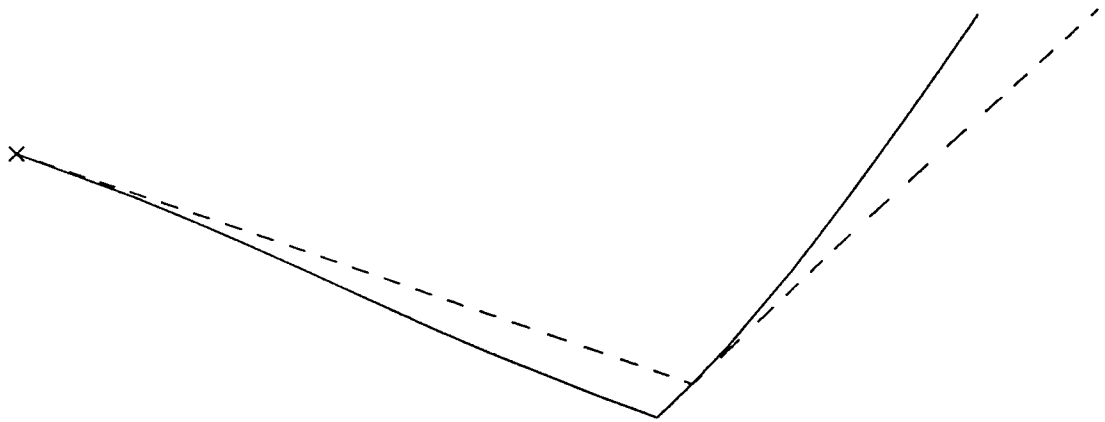

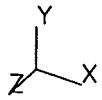

flexarm

LOAD SET: 3 MODE: 3 FREQ: 1.6514057
DISPLACEMENT - NORMAL MIN: 0.00 MAX: 5.02

without piezos

IDEAS FINITE ELEMENT ANALYSIS MODEL

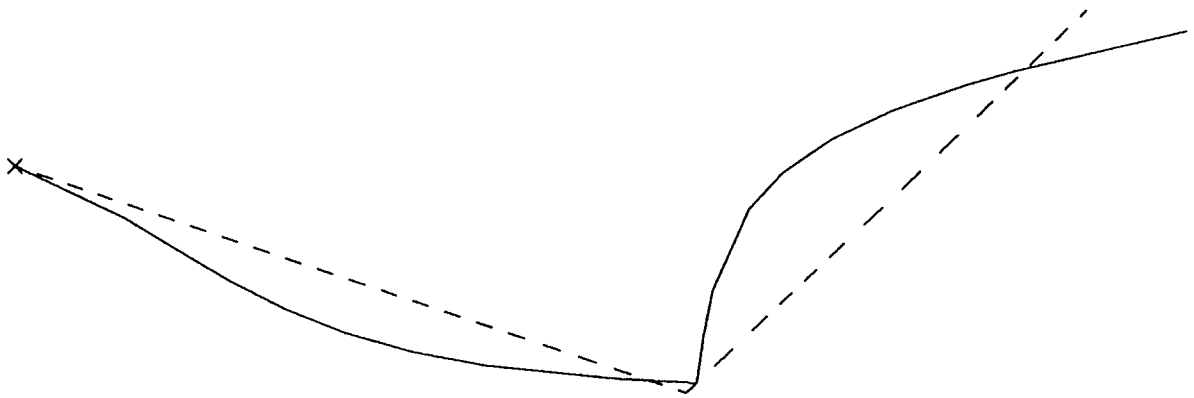

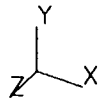

flexarm

LOAD SET: 4 MODE: 4 FREQ: 2.37273
DISPLACEMENT - NORMAL MIN: 0.00 MAX: 5.23

without piežos

IDEAS FINITE ELEMENT ANALYSIS MODEL

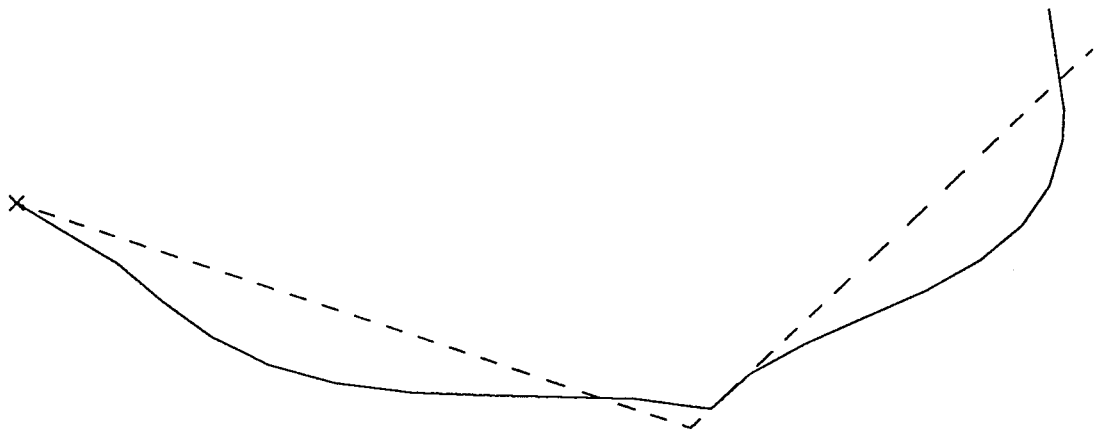

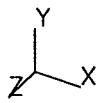

flexarm

LOAD SET: 1 MODE: 1 FREQ: 0.15923978

DISPLACEMENT - NORMAL MIN: 0.00 MAX: 26.83

with piezos

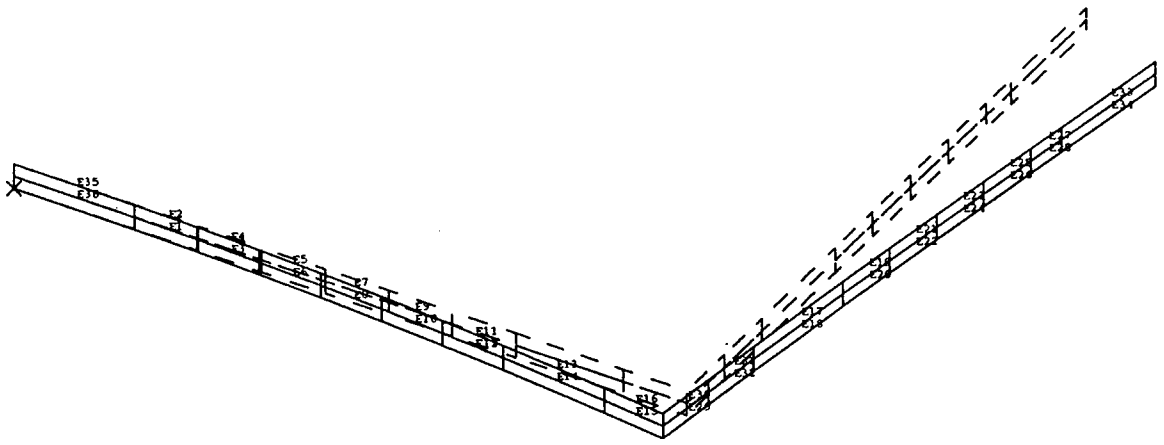

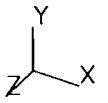

flexarm

LOAD SET: 2 MODE: 2 FREQ: 0.46894449

DISPLACEMENT - NORMAL MIN: 0.00 MAX: 21.13

with piezos

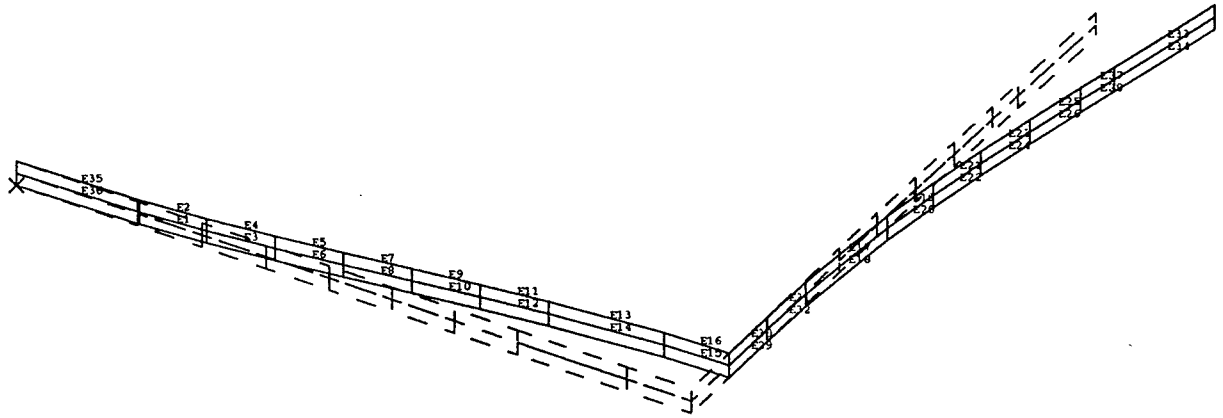

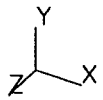

flexarm

LOAD SET: 3 MODE: 3 FREQ: 1.8668766

DISPLACEMENT - NORMAL MIN: 0.00 MAX: 5.25

with piezos

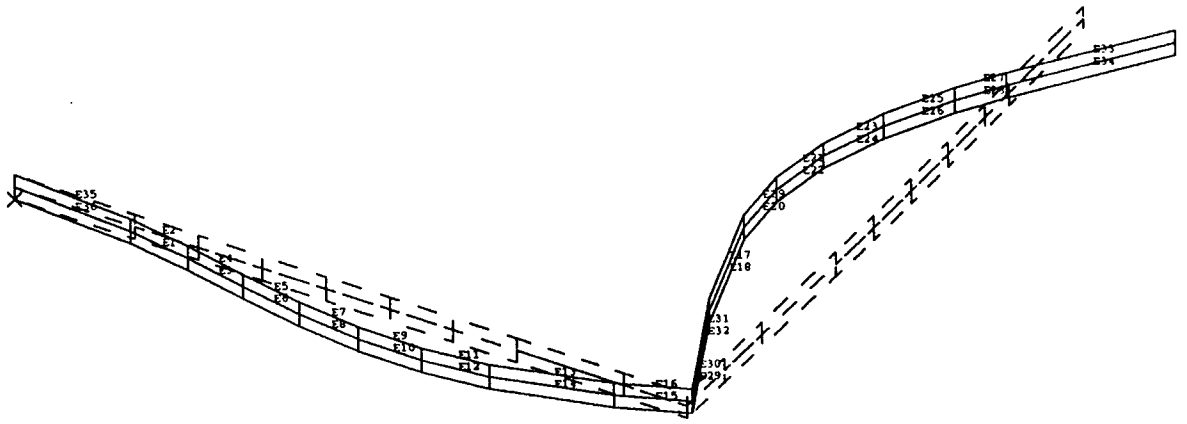

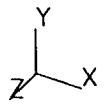

flexarm

LOAD SET: 4 MODE: 4 FREQ: 3.055444

DISPLACEMENT - NORMAL MIN: 0.00 MAX: 6.26

with piezos

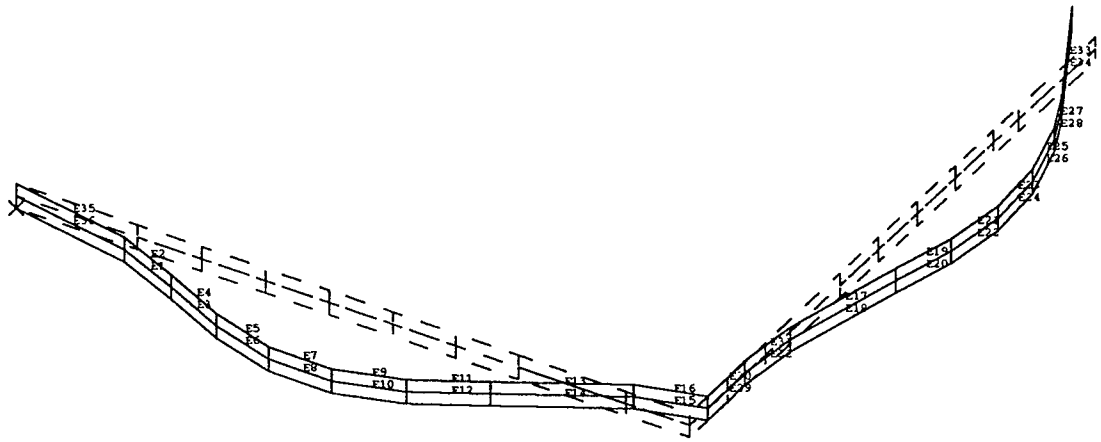

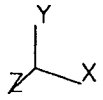

APPENDIX B

```
%  FINITE ELEMENT ANALYSIS OF FSS ARM


clear
m=1.6375e-5;     % Linear Mass Density of Beam in slugs/12/in
mp=2.162e-5;     % Linear Mass Density of Piezo in slugs/12/in

%mp=0;           % no piezo option

h=2.5;
h1=4.75;
h8=4.25;
h12=4.8725;
h17=1.625;
h18=5.0;
                 % beam:

I=2.0345e-5;     % in^4
E=1.0298e7;      % lb/in^2

                 % piezo:

Ip=4.56e-5;      % in^4
Ep=9.137e6;      % lb/in^2


% Mass Intensifiers in slugs/12:
Lma=0.00264;
Lmb=0.0021;
Lmc=0.00472;
Accel=0.000416;

n=18;            %       # of elements


% elemental mass and stiffness

m11=m*h*[156 22*h;22*h 4*h^2]/420;
m22=m*h*[156 -22*h;-22*h 4*h^2]/420;
m12=m*h*[54 -13*h;13*h -3*h^2]/420;
m21=m12';



m22e1=(m+mp)*h1*[156 -22*h1;-22*h1 4*h1^2]/420;
```

```
m11e8=m*h8*[156 22*h8;22*h8 4*h8^2]/420;
m22e8=m*h8*[156 -22*h8;-22*h8 4*h8^2]/420;
m12e8=m*h8*[54 -13*h8;13*h8 -3*h8^2]/420;
m21e8=m12e8';

m11e11=(m+mp)*h*[156 22*h;22*h 4*h^2]/420;
m22e11=(m+mp)*h*[156 -22*h;-22*h 4*h^2]/420;
m12e11=(m+mp)*h*[54 -13*h;13*h -3*h^2]/420;
m21e11=m12e11';

m11e12=m*h12*[156 22*h12;22*h12 4*h12^2]/420;
m22e12=m*h12*[156 -22*h12;-22*h12 4*h12^2]/420;
m12e12=m*h12*[54 -13*h12;13*h12 -3*h12^2]/420;
m21e12=m12e12';

m11e17=m*h17*[156 22*h17;22*h17 4*h17^2]/420;
m22e17=m*h17*[156 -22*h17;-22*h17 4*h17^2]/420;
m12e17=m*h17*[54 -13*h17;13*h17 -3*h17^2]/420;
m21e17=m12e17';

m11e18=(m+mp)*h18*[156 22*h18;22*h18 4*h18^2]/420;
m22e18=(m+mp)*h18*[156 -22*h18;-22*h18 4*h18^2]/420;
m12e18=(m+mp)*h18*[54 -13*h18;13*h18 -3*h18^2]/420;
m21e18=m12e18';

mov=zeros(4);
mov(1:2,1:2)=m22;
mov(2,2)=m22(2,2)+m11e11(2,2);
mov(2,3)=m12e11(2,1);
mov(3,2)=m12e11(2,1);
mov(2,4)=m12e11(2,2);
mov(4,2)=m12e11(2,2);
mov(3:4,3:4)=m22e11;

k11=E*I*[12 6*h;6*h 4*h^2]/h^3;
k22=E*I*[12 -6*h;-6*h 4*h^2]/h^3;
k12=E*I*[-12 6*h;-6*h 2*h^2]/h^3;
k21=k12';

kp1=Ep*Ip*[12 6*h1 -12 6*h1;
          6*h1 4*h1^2 -6*h1 2*h1^2;
          -12 -6*h1 12 -6*h1;
          6*h1 2*h1^2 -6*h1 4*h1^2]/h1^3;

kp2=Ep*Ip*[12 6*h -12 6*h;
```

```
          6*h 4*h^2 -6*h 2*h^2;
          -12 -6*h 12 -6*h;
          6*h 2*h^2 -6*h 4*h^2]/h^3;


                % no piezo option
%kp1=zeros(4);
%kp2=zeros(4);

k22e1=(E*I*[12 -6*h1;-6*h1 4*h1^2]/h1^3)+kp1(3:4,3:4);

k11e8=E*I*[12 6*h8;6*h8 4*h8^2]/h8^3;
k22e8=E*I*[12 -6*h8;-6*h8 4*h8^2]/h8^3;
k12e8=E*I*[-12 6*h8;-6*h8 2*h8^2]/h8^3;
k21e8=k12e8';

k11e11=(E*I*[12 6*h;6*h 4*h^2]/h^3)+kp2(1:2,1:2);
k22e11=(E*I*[12 -6*h;-6*h 4*h^2]/h^3)+kp2(3:4,3:4);
k12e11=(E*I*[-12 6*h;-6*h 2*h^2]/h^3)+kp2(1:2,3:4);
k21e11=k12e11';

k11e12=E*I*[12 6*h12;6*h12 4*h12^2]/h12^3;
k22e12=E*I*[12 -6*h12;-6*h12 4*h12^2]/h12^3;
k12e12=E*I*[-12 6*h12;-6*h12 2*h12^2]/h12^3;
k21e12=k12e12';

k11e17=E*I*[12 6*h17;6*h17 4*h17^2]/h17^3;
k22e17=E*I*[12 -6*h17;-6*h17 4*h17^2]/h17^3;
k12e17=E*I*[-12 6*h17;-6*h17 2*h17^2]/h17^3;
k21e17=k12e17';

k11e18=(E*I*[12 6*h18;6*h18 4*h18^2]/h18^3)+kp1(1:2,1:2);
k22e18=(E*I*[12 -6*h18;-6*h18 4*h18^2]/h18^3)+kp1(3:4,3:4);
k12e18=(E*I*[-12 6*h18;-6*h18 2*h18^2]/h18^3)+kp1(1:2,3:4);
k21e18=k12e18';

kov=zeros(4);
kov(1:2,1:2)=k22;
kov(2,2)=k22(2,2)+k11e11(2,2);
kov(2,3)=k12e11(2,1);
kov(3,2)=k12e11(2,1);
kov(2,4)=k12e11(2,2);
kov(4,2)=k12e11(2,2);
kov(3:4,3:4)=k22e11;
```

```
% global mass matrix

gm(1:2,1:2)=m22e1+m11;
gm(1:2,3:4)=m12;

for i=1:n-2


      gm(2*i+1:2*i+2,2*i-1:2*i)=m21;
      gm(2*i+1:2*i+2,2*i+1:2*i+2)=m22+m11;
      gm(2*i+1:2*i+2,2*i+3:2*i+4)=m12;

end

gm(17:20,17:20)=mov;

gm(13:14,13:14)=m22+m11e8;
gm(15:16,13:14)=m21e8;
gm(13:14,15:16)=m12e8;
gm(15:16,15:16)=m22e8+m11;

gm(19:20,19:20)=m22e11+m11e11;
gm(21:22,19:20)=m21e11;
gm(19:20,21:22)=m12e11;
gm(21:22,21:22)=m22e11+m11e12;

gm(23:24,21:22)=m21e12;
gm(21:22,23:24)=m12e12;
gm(23:24,23:24)=m22e12+m11;

gm(31:32,31:32)=m22+m11e17;
gm(33:34,31:32)=m21e17;
gm(31:32,33:34)=m12e17;
gm(33:34,33:34)=m22e17+m11e18;

gm(35:36,33:34)=m21e18;
gm(33:34,35:36)=m12e18;
gm(35:36,35:36)=m22e18;

Lmm=zeros(size(gm));
Lmm(3,3)=Lma;
Lmm(5,5)=Lma;
Lmm(7,7)=Lma;
Lmm(9,9)=Lma;
```

```
Lmm(11,11)=Lma;
Lmm(13,13)=Lma;
Lmm(23,23)=Lma;
Lmm(25,25)=Lma;
Lmm(29,29)=Lma;
Lmm(31,31)=Lma;
Lmm(27,27)=Accel;
Lmm(17,17)=Lmb+0.0154;
Lmm(35,35)=Lmc;
gmm=gm+Lmm;

% global stiffness matrix

gk(1:2,1:2)=k22e1+k11;
gk(1:2,3:4)=k12;

for i=1:n-2

        gk(2*i+1:2*i+2,2*i-1:2*i)=k21;
        gk(2*i+1:2*i+2,2*i+1:2*i+2)=k22+k11;
        gk(2*i+1:2*i+2,2*i+3:2*i+4)=k12;

end

gk(17:20,17:20)=kov;

gk(13:14,13:14)=k22+k11e8;
gk(15:16,13:14)=k21e8;
gk(13:14,15:16)=k12e8;
gk(15:16,15:16)=k22e8+k11;

gk(19:20,19:20)=k22e11+k11e11;
gk(21:22,19:20)=k21e11;
gk(19:20,21:22)=k12e11;
gk(21:22,21:22)=k22e11+k11e12;

gk(23:24,21:22)=k21e12;
gk(21:22,23:24)=k12e12;
gk(23:24,23:24)=k22e12+k11;

gk(31:32,31:32)=k22+k11e17;
gk(33:34,31:32)=k21e17;
gk(31:32,33:34)=k12e17;
gk(33:34,33:34)=k22e17+k11e18;

gk(35:36,33:34)=k21e18;
```

```
gk(33:34,35:36)=k12e18;
gk(35:36,35:36)=k22e18;


% mode shapes and natural freqs

B=inv(gmm)*gk;
[x,D]=eig(B);
w=sqrt(D);
f=w/2/pi;
[k1,k2]=sort(diag(D));
x=x(:,k2);

% modal masses

y=x'*gmm*x;

% mode shapes normalized wrt mass

for i=1:2*n

        z(:,i)=x(:,i)/sqrt(y(i,i));

end
z;
```

```
» fea
» diag (f)

ans =

   1.0e+003 *

    4.59118474609514
    3.99568135727380
    3.59480701359855
    2.99704503076688
    2.93678510562751
    2.28716854586410
    2.12001248476245
    2.00095892851113
    1.64377826366426
    1.57337814606062
    1.36667629704302
    1.24571931505966
    1.13139307876285
    1.08173078771907
    0.83137661757685
    0.80808968513644
    0.67562468034393
    0.65960922618500
    0.33282677547923
    0.22223482048505
    0.20688050862119
    0.18556683346412
    0.11445097218405
    0.09656670691812
    0.06764056549358
    0.04693032740926
    0.03658424100849
    0.02811923523049
    0.02120575875813
    0.01459733742682
    0.00694405426306
    0.00599862204817
    0.00237295384752
    0.00164563740851
    0.00037335596675
    0.00013563176832

»
```

APPENDIX C

Modal Frequencies (without piezos), descending order

```
» diag(f)

ans =

  1.0e+003 *

   4.48533942414282
   4.20598887360221
   3.93601883252608
   2.95655175921535
   2.91232463252813
   2.40665996231507
   2.12840833617064
   2.01547862614741
   1.67501528412810
   1.61012336453201
   1.39849731540630
   1.27385368688073
   1.14741402755860
   1.10615287290734
   0.85542324830144
   0.83293574716167
   0.72369166064969
   0.68994155774074
   0.34608426976888
   0.22304670115122
   0.22787352029346
   0.18559636091107
   0.11394978872364
   0.08854986624844
   0.06796197347123
   0.04772133056046
   0.03761481660823
   0.02913274059718
   0.02217253369177
   0.01562031009177
   0.00771814099641
   0.00652352892696
   0.00285149622307
   0.00178656363092
   0.00046041550163
   0.00016213258818

»
```

Modal Frequencies (with piezos), descending order

APPENDIX D. MODAL TESTING HARDWARE

A. ACCELEROMETER

1. Model

Sensotec Model # 3629-05

2. Available Ranges

+/- 10g

3. Sensitivity

10 mV/g

4. Usable Frequency (Bandwidth)

0-250 Hz

5. Excitation

+/- 5V

B. SIGNAL CONDITIONER

1. Model

Instruments Division Measurement Group, Inc. Model 2100

2. Type

Strain Gage Conditioner and Amplifier System with Integral Power Supply

3. Gain

1-2100

4. Operation

Full Balanced Operation for Noise Rejection

C. IMPULSE FORCE HAMMER

1. Model

PCB Piezotronics Model # 086B01

2. Range

0-100 Lb.

3. Hammer Sensitivity

52.2 mV/g

D. HAMMER POWER SUPPLY

PCB Piezotronics Model # 483B03 Line Power Supply

E. DATA ACQUISITION HARDWARE

Hewlett-Packard Model HP 3565S Measurement/Data Acquisition System

LIST OF REFERENCES

1. Newman, S., *Active Damping Control of a Flexible Space Structure Using Piezoelectric Sensors and Actuators*, Master's Thesis, Naval Postgraduate School, Monterey, California, 1992.

2. Feuerstein, M.G., *A Comparison of Different Control Methods for Vibration Suppression of Flexible Structures Using Piezoelectric Actuators,* Master's Thesis, Naval Postgraduate School, Monterey, California, 1994.

3. Inman, D.J., *Vibration: With Control, Measurement, and Stability,* Prentice Hall, Englewood Cliffs, New Jersey, 1989.

4. Meirovitch, L., *Elements of Vibration Analysis,* McGraw-Hill, Inc., New York, New York, 1986.

5. Betros, R.S., and Bronowicki, A.J., "Seminar Notes", *Active Damping Workshop,* Spring, 1991.

6. Hanagud, S., Obal, M.W., and Calise, A.J.,"Optimal Vibration Control by the Use of Piezoceramic Sensors and Actuators", *Journal of Guidance, Control, and Dynamics,* Vol. 15, No. 5, Sept-Oct, 1992, pp. 1199-1206.

7. Ewins, D.J., *Modal Testing: Theory and Practice,* Research Studies Press Ltd., John Wiley, New York, New York, 1984.

8. Structural Data Research Corporation, *I-DEAS™ Test User's Guide,* Milford, Ohio, 1990.

9. James, M.L., Smith, G.M., Wolford, J.C., and Whaley, P.W., *Vibration of Mechanical and Structural Systems with Microcomputer Applications,* Harper and Row, Publishers, Inc., New York, New York, 1989.

INITIAL DISTRIBUTION LIST

	Number of Copies
1. Defense Technical Information Center Cameron Station Alexandria, Virginia 22304-6145	2
2. Library, Code 52 Naval Postgraduate School Monterey, California 93943-5104	2
3. Chairman, Code AA Department of Aeronautics and Astronautics Naval Postgraduate School Monterey, California 93943-5002	1
4. Chairman, Code SP Department of Aeronautics and Astronautics Naval Postgraduate School Monterey, California 93943-5002	1
5. Commander, Naval Space Command Attn: N112 5280 4th Street Dahlgren, Virginia 22448-5300	1
6. Professor Brij N. Agrawal, Code AA/Ag Department of Aeronautics and Astronautics Naval Postgraduate School Monterey, California 93943-5002	2
7. Professor Hyochoong Bang, Code AA/Ba Department of Aeronautics and Astronautics Naval Postgraduate School Monterey, California 93943-5002	1
8. CDR James C. Trump, USN 6539 Corintia Street Carlsbad, California 92009	1